JOURNAL OF AIRCRAFT
Vol. 44, No. 2, March–April 2007

Flight Control Using Synthetic Jets on a Cessna 182 Model

Marcus Ciuryla*
Rensselaer Polytechnic Institute, Troy, New York 12180
Yong Liu†
Ohio University, Athens, Ohio 45701
John Farnsworth‡
Rensselaer Polytechnic Institute, Troy, New York 12180
Chiman Kwan§
Intelligent Automation, Inc., Rockville, Maryland 20855
and
Michael Amitay¶
Rensselaer Polytechnic Institute, Troy, New York 12180

DOI: 10.2514/1.24961

The application of active flow control via synthetic jet actuators for separation and roll control on a scaled Cessna 182 model was investigated experimentally in a low-speed wind tunnel. The model was instrumented with either ailerons or synthetic jets embedded within the outer portion of the wings' span, in lieu of ailerons. Force and moment measurements were performed for various aileron deflections and synthetic jet momentum coefficients (on either both wingtips or only on one). It was found that the effectiveness of the synthetic jets is comparable to that of conventional ailerons at moderate deflection angles. The model was also instrumented with a hot-film shear stress sensor downstream from the synthetic jet exit. The sensor's rms output was monitored in real time by a computer. When the rms reached a predetermined threshold value, the computer automatically turned on the synthetic jet actuators. Using the appropriate threshold value resulted in complete avoidance of wingtip stall at the angle of attack where separation would have occurred. In addition, the shear stress sensor and wind tunnel force data were used to identify the system dynamics. A computerized dynamic model of an RC version of the Cessna 182 showed that at moderate to high angles of attack, synthetic jets alone could be used to control the roll of the aircraft.

Nomenclature

b	=	wing span
C_D	=	vehicle drag coefficient
C_L	=	vehicle lift coefficient
C_m	=	vehicle pitching moment (about quarter-chord)
C_{m_α}	=	derivative of C_m with respect to the angle of attack
C_n	=	vehicle yaw moment coefficient (about quarter-chord and center plane)
C_r	=	vehicle rolling moment coefficient
C_μ	=	synthetic jets' momentum coefficient, $(n_j \rho_j U_j^2 h L_j)/(\frac{1}{2}\rho_\infty U_\infty^2 \bar{c} b)$
$\bar{c}$	=	mean chord
$f_r(V)$, $f_n(V)$	=	coefficients listed in Eqs. (4) and (5)
g	=	acceleration due to gravity
h	=	synthetic jet orifice width
L_j	=	synthetic jet orifice length
m	=	mass
n_j	=	number of active synthetic jets
Re	=	Reynolds number, $(U_\infty \bar{c})/\nu$
T	=	reattachment time constant
T_f	=	time of flight, $\bar{c}/U_\infty$
T_j	=	synthetic jet period
t	=	time
U_j	=	synthetic jet orifice velocity (during the outstroke), $\frac{1}{T_j}\int_0^\tau u_j(t)\,\mathrm{d}t$
U_∞	=	freestream velocity
u_b	=	x-component of inertial velocity in airplane body frame F_B
$u_j(t)$	=	phase-averaged velocity at the jet exit plane
V	=	input voltage to the synthetic jets (before amplification)
w_b	=	z-component of inertial velocity in airplane body frame F_B
x_{sj}	=	streamwise location of the synthetic jet actuators
α	=	angle of attack
ΔC_r	=	change in rolling moment coefficient with respect to aileron deflection of 3 deg
$\Delta C_{r_{\mathrm{sj}}}$	=	change in rolling moment coefficient from synthetic jet configuration (jets off)
δ_a	=	aileron deflection
δ_E	=	elevator command
δ_R	=	rudder command
δ_{SV}	=	synthetic jet command
δ_{Th}	=	engine command
λ	=	closed-loop control system characteristics root
ρ_j	=	synthetic jet density
ρ_∞	=	freestream fluid density
τ	=	synthetic jet blowing time, $T_j/2$

Received 4 May 2006; revision received 1 August 2006; accepted for publication 11 August 2006.

*Graduate student, Mechanical, Aerospace and Nuclear Engineering Department.
†Graduate student, School of Electrical Engineering and Computer Science. Student Member AIAA.
‡Undergraduate student, Mechanical, Aerospace and Nuclear Engineering Department. Student Member AIAA.
§Vice President, 15400 Calhoun Drive, Suite 400.
¶Assistant Professor, Mechanical, Aerospace and Nuclear Engineering Department; amitam@rpi.edu (corresponding author). Senior Member AIAA.

Introduction

OPTIMUM aerodynamic performance that avoids flow separation on wing surfaces has been traditionally achieved by appropriate aerodynamic design of airfoil sections. However, when the wing design is driven by nonaerodynamic constraints (stealth, payload, etc.), the forces and moments of the resulting unconventional airfoil shape may be much smaller than a conventional airfoil. Therefore, either active or passive flow control can be used to maintain aerodynamic performance throughout the normal flight envelope. Although passive control devices such as vortex generators have proven, under some conditions, to be quite effective in delaying flow separation, they offer no proportional control and introduce a drag penalty when the flow does not separate (or when they are not needed) [1].

In contrast, active control enables coupling of the control input to flow instabilities that are associated with flow separation and thus may enable substantial control authority at low actuation levels. Furthermore, active actuation is largely innocuous except when activated and has the potential for delivering variable power. In previous studies, active control efforts have employed a variety of techniques including external and internal acoustic excitation [2–4], vibrating ribbons or flaps [5], and steady or unsteady blowing [6].

Over the last decade, the synthetic jet has emerged as a versatile actuator for active flow control. The formation and evolution of synthetic jets are described in detail in the work of Smith and Glezer [7], Amitay and Glezer [8], and Amitay and Cannelle [9]. The effectiveness of fluidic actuators based on synthetic jets is derived from the interaction of these jets with the flow near the flow boundary that can lead to the formation of a quasi-closed recirculating flow region, resulting in a virtual modification in the shape of the surface. Past research work has focused on the use of open-loop actuation strategies to generate the required modulated input signals to jet arrays [6,10–12], which is highly dependent on the availability of accurate and comprehensive wind-tunnel-validated flow models. However, the underlying flow mechanisms and interactions of jet arrays are usually very complicated and highly nonlinear. Moreover, it is extremely difficult to accurately model the changes in the system dynamics due to varied flight conditions, inevitable external disturbances, measurement noise, actuator anomalies, and failures. Therefore, the development of closed-loop nonlinear adaptive flow control techniques that can automatically compensate for modeling errors and adapt to changes in the system dynamics, are particularly attractive to realize the full potential of synthetic jet technology.

Recently, the effect of synthetic jets on a scaled model of a Piper J-3 Cub was examined [13] at Reynolds numbers from 150,000 to 280,000. Increases in total vehicle lift of up to 16% were observed. A dynamic analysis on the Piper showed that synthetic jets had only a minor influence on stability characteristics, and that the effect was greater at high angles of attack. The previous work also showed that synthetic jets on the main wing of an aircraft could be used to control the pitch of the aircraft to a modest extent.

The present work has three objectives: 1) to explore, experimentally, the feasibility of using active flow control, via synthetic jet actuators, as a roll control mechanism instead of conventional ailerons for the small-scale Cessna 182 model; 2) to develop a closed-loop stall suppression system on a wind tunnel model of the Cessna 182; and 3) to develop an integrated flight controller (body rate controller) for the RC Cessna flying model, instrumented with synthetic jet wingtips.

Experimental Setup

The experiments were conducted in a closed-return low speed wind tunnel, having a test section measuring 608 by 608 mm, which is equipped with a six-component force sting balance to measure the aerodynamic forces and moments. All forces and moments reported in the paper are about the quarter-chord of the wing along the model centerline. The resolution of the sting balance was such that the moments and forces were measured with an accuracy of less than 5%. The experiments were conducted at 15 and 30 m/s, with a corresponding Reynolds number of 67,300 and 134,600, respectively, and (wing) angles of attack from 0 to 16 deg. The uncertainty in the velocity is less than 1% whereas the angle of attack alignment is within 0.1 deg.

A 1/24th Cessna scaled model (457 mm span) was constructed from stereolithography, where the main wing consists of a NACA 2412 section, and a NACA 0005 was used for both the horizontal and vertical tails. The main wing was designed such that different wingtips could be used (Fig. 1) where aileron deflections from 0 to 18 deg in 3 deg increments could be achieved. Note that each aileron's streamwise length is 20% of the root chord on the outer span portions (25% of the span for each aileron) of the wing.

In addition to the aileron deflection wingtips, several wingtips with embedded synthetic jets were also designed (Fig. 1b). A synthetic jet is a jet that is synthesized by a train of two-dimensional vortex pairs. The vortices are formed at the edge of an actuator orifice by the motion of a small diaphragm that is driven by a piezoceramic disc and mounted at the bottom of a sealed shallow cavity. During the forward motion of the diaphragm, fluid is ejected from the cavity, and the ensuing flow separates at the sharp edge of the orifice forming two vortex sheets that roll into a vortex pair that begins to move away from the orifice under its own self-induced velocity. When the diaphragm begins to move away from the orifice, the vortex is sufficiently removed and is thus unaffected by the ambient fluid that is drawn into the cavity. Therefore, during each cycle the net mass flux out of the cavity is zero whereas the hydrodynamic impulse of each vortex is nonzero. The diaphragm is driven at its resonance and thus the electrical power input to the actuator is typically small. Furthermore, the synthetic jet is very simple mechanically and does

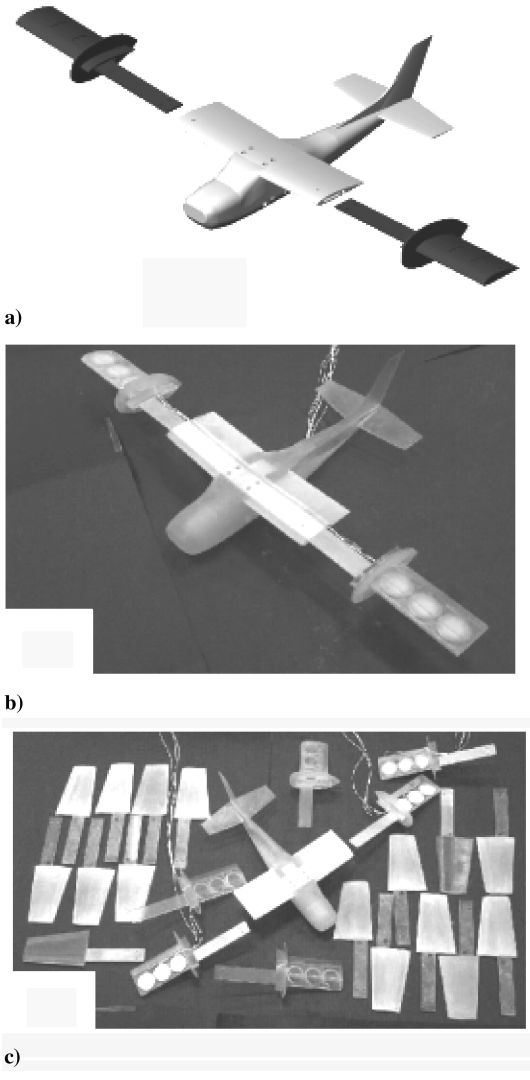

Fig. 1 Cessna wind tunnel model.

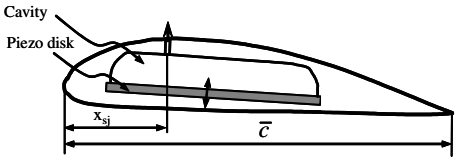

Fig. 2 Cross section schematics of the wingtip instrumented with synthetic jet actuators.

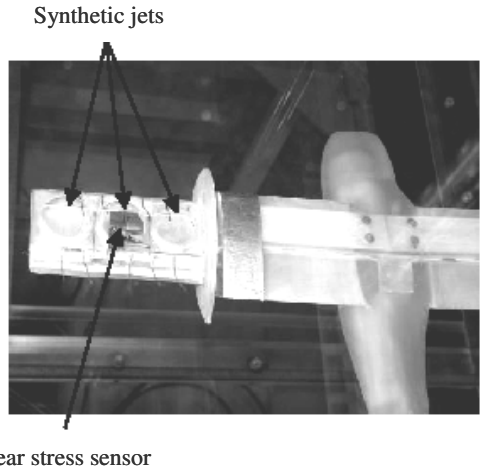

Fig. 3 Cessna model with synthetic-jets-instrumented wingtip.

not require compressed air or tubing. For a detailed description of the synthetic jet see the review by Amitay and Glezer [8]. In the present work the synthetic jet was mounted at $x_{sj}/\bar{c} = 0.25$ (near the separation point for high angles of attack, Fig. 2), and its synthetic jet performance was measured using the momentum coefficient, C_μ, which was varied between 1.5×10^{-4} and 8.7×10^{-3} (when both wingtips are actuated) and between 7.4×10^{-5} and 4.3×10^{-3} (when a single wingtip is actuated).

The baseline Cessna has a small taper over the aileron portion of the span. However, to avoid any three-dimensional taper effects, the synthetic jet wingtips were designed without any taper ($\bar{C} = 67$ mm), but with the same planform area and overall span as the aileron wingtips. The synthetic jet-instrumented wingtips have an 18% thick Clark-Y airfoil section (the effect of flow control, via synthetic jet actuators, on a 2-D Clark-Y airfoil was previously investigated by Amitay et al. [14]). A thicker airfoil (than the baseline wingtip) was chosen to provide enough room for the synthetic jet cavities. Moreover, a stall fence was added to the synthetic jet wingtips to prevent any tip effects from imposing on the inner span of the wing. Each wingtip consists of 3 synthetic jets (at the 25% chord location and 7.5 mm apart, Fig. 3) each having a 0.5 mm wide slit and extending 25.4 mm along the span. Each synthetic jet actuator is driven at a frequency of 750 Hz using a piezoceramic disk. In addition, a hot-film shear stress sensor was placed downstream the synthetic jet exit (at 35% chord, Fig. 3).

Results

The implementation of synthetic jet actuators for separation control and as ailerons for roll control on a scaled Cessna 182 model has been investigated experimentally. First, the baseline configuration is discussed, where ailerons are used for roll. Following, the effectiveness of synthetic-jets-based active flow control instead of the ailerons is presented, and finally, the development of an integrated flight controller for an RC Cessna flying model, which is instrumented with synthetic jets wingtips, is shown.

Aileron Configuration

First, the aerodynamic performance of the baseline Cessna model (i.e., with conventional ailerons) is presented. Figures 4a and 4b present the variation of the vehicle's lift coefficient, CL, with angle of attack and the lift-drag polar, respectively. The data are at $Re = 67,300$ and 134,600 and four aileron deflection angles. The lift coefficient increases linearly for $\alpha < 8$ deg and reaches its maximum value, $C_{L\max}$, of 1.2 at $\alpha = 11$ deg (Fig. 4a). As expected, the lift coefficient is not noticeably affected by aileron deflection. However, the drag coefficient increases slightly with increasing aileron deflection (Fig. 4b). Furthermore, there is no noticeable effect due to Reynolds number at this range of Reynolds numbers.

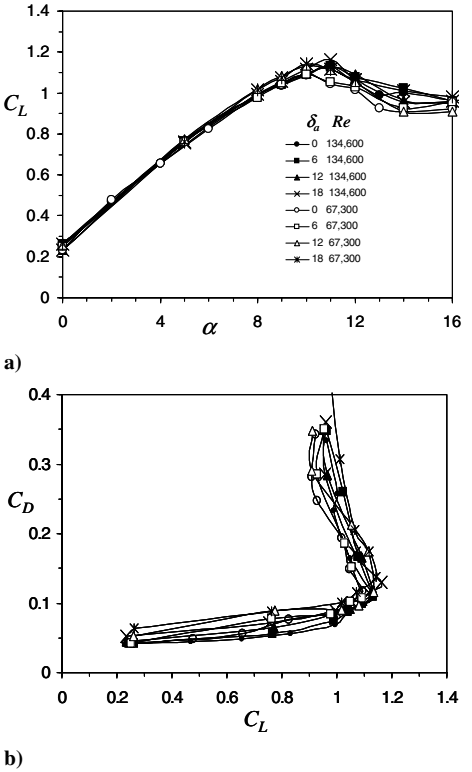

Fig. 4 a) Lift coefficient vs angle of attack; b) drag polar for the baseline Cessna.

The pitching moment characteristics for the baseline configuration were also measured and the change of the pitching moment (about the wing's quarter-chord) with the angle of attack is presented in Fig. 5. As expected, the moment on the entire vehicle is negative (e. g., stable vehicle), where the moment coefficient increases (i.e., becomes more negative) linearly with angle of attack (the derivative of C_m with respect to the angle of attack, C_{m_α}, is -0.037 per degree).

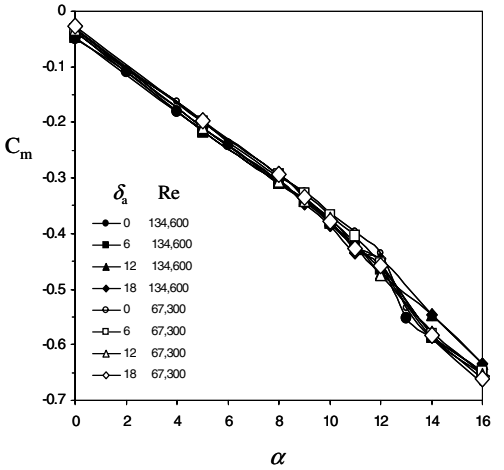

Fig. 5 Pitching moments vs angle of attack at different aileron deflections.

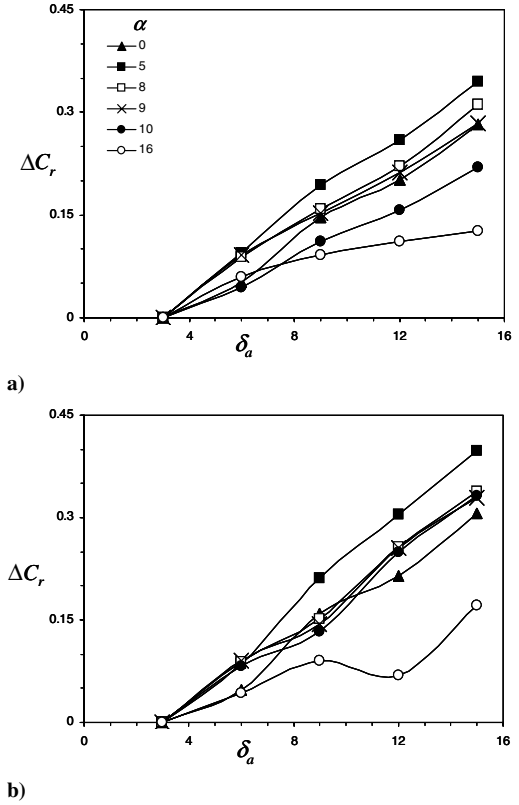

Fig. 6 Change of the roll moment (with respect to the value at $\delta_a = 3$ deg) vs the deflection angle at different angles of attacks; a) $Re = 67,300$ and b) 134,600.

Similar to the earlier results, neither the Reynolds number nor the aileron deflection angle has a meaningful effect on C_m.

Next, the change in the roll coefficient with the aileron deflection is presented in Figs. 6a and 6b for $Re = 67,300$ and 134,600, respectively. Here, the roll coefficient at an aileron deflection angle of 3 deg (for each angle of attack) is subtracted from the roll coefficient such that at $\delta_a = 3$ deg, $\Delta C_r = 0$ for all angles of attack. This representation makes it easy to display the effect of aileron deflection on C_r for different α. The effects are similar at both Reynolds numbers tested; for a given α, as the aileron deflection increases, the rolling moment also increases. For low to moderate angles of attack ($\alpha < 9$ deg) the increase of C_r with δ_a is the largest (and it is linear). At $\alpha > 9$ deg the flow over the wing separates, resulting in a decrease in aileron effectiveness.

To properly formulate a mathematical dynamic model of the vehicle, the relationship between the rolling moment and the aileron deflection is needed. Therefore, the data for angles of attack from 0 to 9 deg are replotted and a linear fit found to be the best fit for the data where $\mathrm{d}(\Delta C_r)/\,\mathrm{d}\delta_a = 0.025$ (Fig. 7). Note that these data are used to develop the dynamic model of the vehicle.

Synthetic Jet Configuration

Next, the effect of flow control, via synthetic jet actuators, on flow separation and roll control was investigated and is presented in this section. Figure 8a shows the effect of the momentum coefficient of the synthetic jets, C_μ, on the lift coefficient at different angles of attack and for $Re = 67,300$. For low angles of attack ($\alpha < 3$ deg) there is hardly any effect of flow control (the flow is fully attached over the wingtips, whereas for higher angles of attack the activation of the synthetic jets results in an increase in the lift coefficient, even at C_μ as low as 5.8×10^{-4}). Note that for $3 < \alpha < 6$ deg the flow on the wingtips is partially separated; thus, the effect of the control is the same regardless of the momentum coefficient. However, at moderate to high angles of attack, where the flow is massively separated (on the entire wing) the effect of the momentum coefficient is clearly visible: as C_μ increases the lift coefficient increases, suggesting that

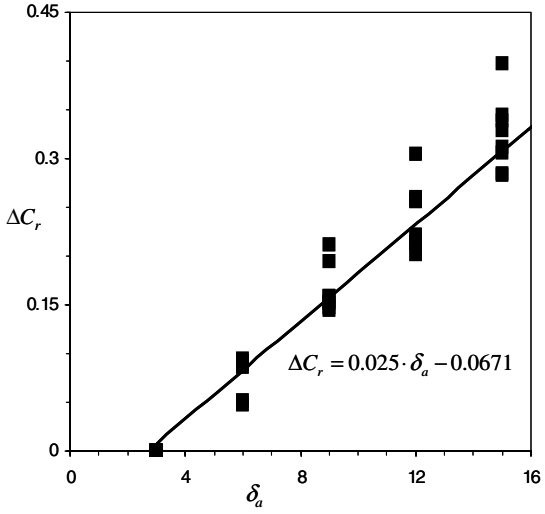

Fig. 7 Change of the roll moment (with respect to the value at $\delta_a = 3$ deg) vs the deflection angle for $5 \le \alpha \le 9$ deg.

proportional control can be achieved. This is very important if closed-loop control is to be implemented.

As mentioned before, the airfoil used for the synthetic jet wingtips is 18% thick Clark-Y, which does not have the same aerodynamic performance as the baseline airfoil (NACA 2412). Thus, it is expected that the lift coefficient of the Cessna will be smaller when the synthetic-jet-instrumented wingtips are used (without flow control) as shown in Fig. 8b. Figure 8b presents a comparison of the lift coefficient (for different angles of attack) for the baseline (aileron) configuration, and the synthetic jet configuration (with and without activation of the synthetic jets). Without activation of the

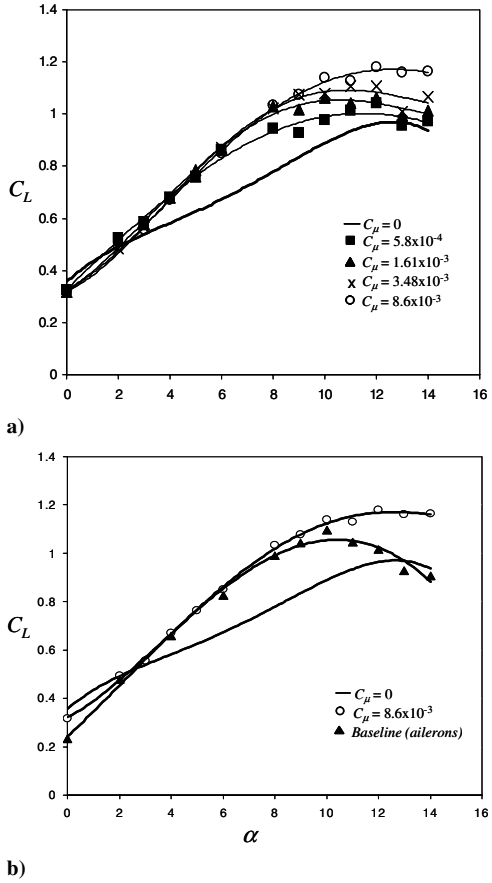

Fig. 8 Lift coefficient vs angle of attack; a) synthetic jets wingtips and b) comparison with the baseline Cessna. $Re = 67,300$.

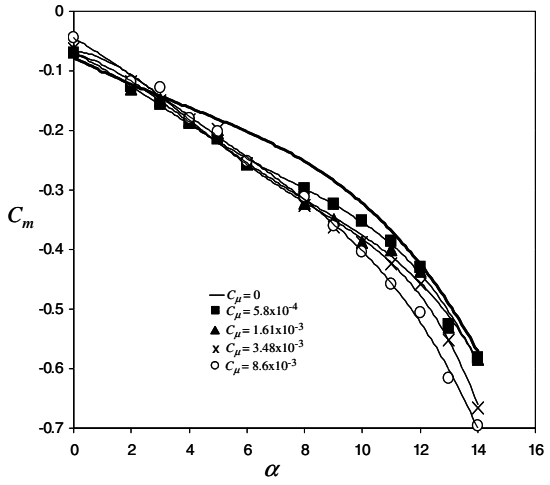

Fig. 9 Pitching moments vs angle of attack at different momentum coefficients.

jets, the lift coefficient of the synthetic jet configuration has worse performance than the baseline configuration for $\alpha > 2$ deg. When the synthetic jets are activated (with $C_\mu = 8.6 \times 10^{-3}$) the lift coefficient is recovered (to the baseline values) for $\alpha < 6$ deg whereas for $\alpha > 6$ deg the lift coefficient surpasses the baseline values by up to 15%. Furthermore, the stall angle is increased by ~ 2 deg.

The effect of flow control on the pitching moment coefficient was also measured as a function of the angle of attack and is presented in Fig. 9 for various synthetic jet momentum coefficients. There is a definite trend that as the momentum coefficient is increased, the vehicle moment coefficient is more negative (i.e., more stable vehicle). Moreover, proportional pitching control is obtained for $\alpha > 6$ deg.

In the data presented in Figs. 8 and 9 the synthetic jets on both wingtips were activated; however, to obtain a rolling moment the synthetic jets on either the left or the right wingtip were activated separately. Figure 10 shows the change in the roll coefficient (with respect to the corresponding values when the synthetic jets are not activated) with the synthetic jet momentum coefficient. The dashed lines correspond to the starboard synthetic jets activated, and the solid lines represent the port synthetic jets activated. At $\alpha = 0$ deg a very small roll moment is obtained and it is similar for all the momentum coefficients that were tested. When the angle of attack is increased to 6 deg proportional control is obtained, where as C_μ increases ΔC_r decreases. Note that similar trends were obtained at all

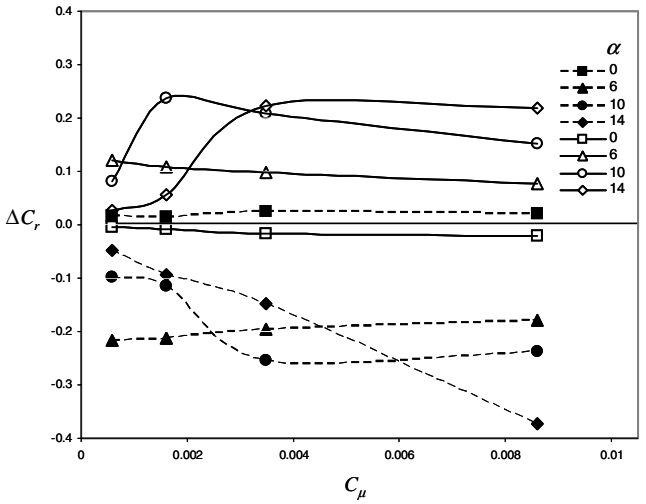

Fig. 10 Change of the roll moment (with respect to the unforced case) vs the momentum coefficient at different angles of attack. The dashed lines correspond to the starboard synthetic jets activated whereas the solid lines represent the port synthetic jets activated.

angles between 5 and 9 deg, and the 6 deg is shown here as a representative case. At higher angles of attack, where the flow is completely separated over the wingtips (without flow control), the effect of the momentum coefficient is different. At $\alpha = 10$ deg, for low C_μ, increase in C_μ yields a higher rolling moment whereas for $C_\mu > 1.73 \times 10^{-3}$, as C_μ increases ΔC_r decreases. At angles of attack past the stall angle, low momentum coefficient is not sufficient to reattach the flow over the wingtip and thus low rolling moment is achieved. However, high momentum coefficient jets can reattach the flow and create a rolling moment. It is noteworthy that the magnitudes of the rolling moments obtained with synthetic jet actuators is similar to those obtained with ailerons at deflection angles of 12 deg and smaller.

Closed-Loop Active Stall Suppression

In this section a simple closed-loop control is used to suppress separation over the wingtips using a dynamic shear stress sensor to detect the separation and synthetic jet actuators to reattach the flow. The separation was observed qualitatively, using tuft flow visualization, and detected quantitatively, using the shear stress sensor. Figures 11a and 11b present the time trace of the shear stress sensor output voltage, and the tuft visualization over the wingtip, respectively, at $\alpha = 0$ deg. At this low angle of attack the flow is completely attached over the wingtip as indicated by the tufts and the very low rms shear stress sensor output. Note that the shear stress sensor was not calibrated and is used here only to detect separation based on the rms of its output signal.

As the angle of attack is increased to $\alpha = 8.5$ deg the flow over the wingtips is separated as indicated by the high rms values from the shear stress (Fig. 12a) and confirmed by the tufts, which clearly show reversed flow over parts of the wingtip (Fig. 12b). The time trace of the shear stress sensor exhibits two main frequencies of ~ 10 and ~ 100 Hz, which correspond to the model vibration and the shedding frequency of the separated flow over the wingtip, respectively. Note that visual examination of the wingtips at these conditions confirmed the buffeting of the wingtips, without flow control.

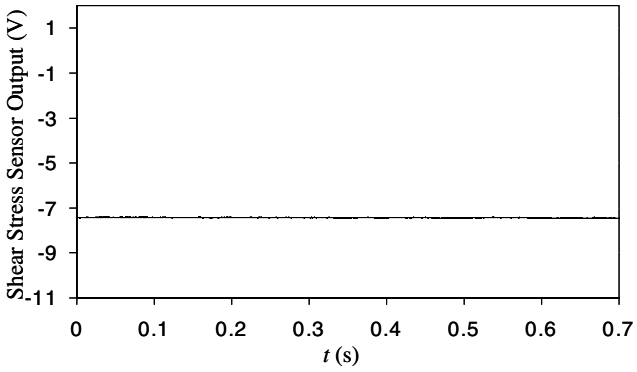

a)

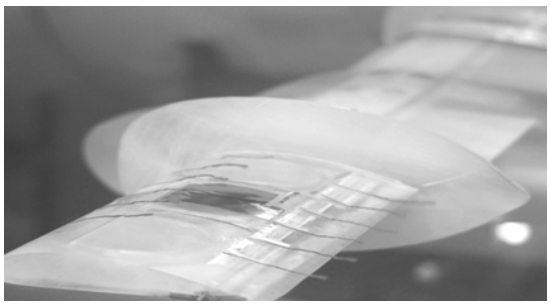

b)

Fig. 11 a) Time trace of the shear stress sensor output; b) tufts flow visualization over the wingtip. $\alpha = 0$ deg, synthetic jets off.

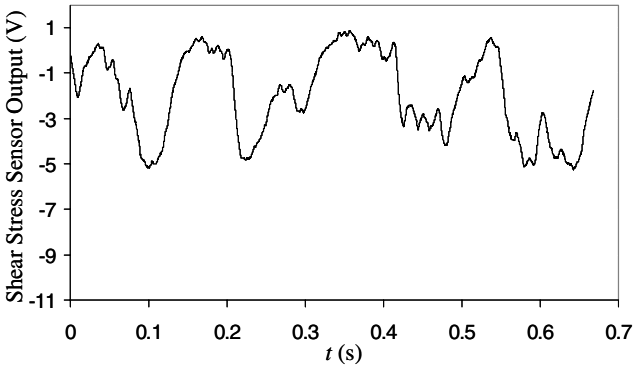

a)

b)

Fig. 12 a) Time trace of the shear stress sensor output; b) tufts flow visualization over the wingtip. $\alpha = 8.5$ deg, synthetic jets off.

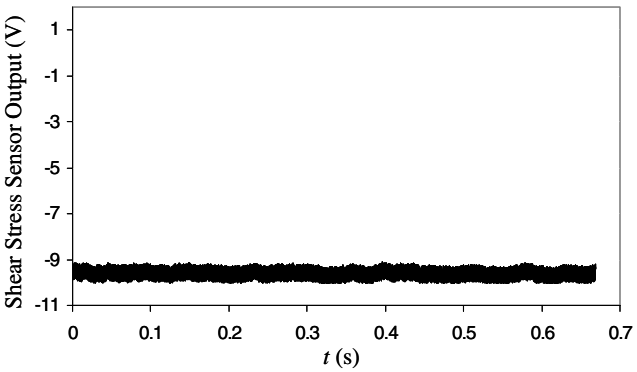

a)

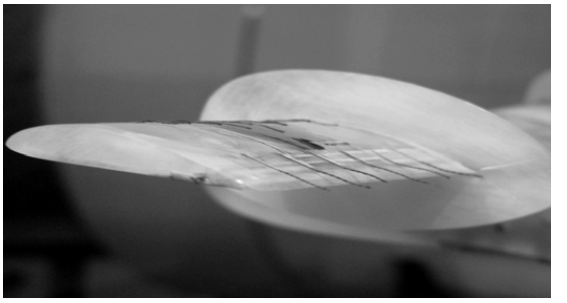

b)

Fig. 13 a) Time trace of the shear stress sensor output; b) tufts flow visualization over the wingtip. $\alpha = 8.5$ deg, synthetic jets on ($C_\mu = 8.6 \times 10^{-3}$).

When the synthetic jets are activated with $C_\mu = 8.6 \times 10^{-3}$ the flow is completely reattached as indicated by the low rms levels of the shear stress sensor (Fig. 13a) and the tufts (Fig. 13b). Note the presence of the low-amplitude periodic oscillations in the shear stress sensor signal at the synthetic jets actuation frequency, due to its proximity to the synthetic jet actuators. Moreover, the actuation of the synthetic jet eliminated completely the low frequency model vibrations (as was visually confirmed). Also, in the anemometry system used in these experiments, decrease in the output voltage of the sensor corresponds to increase in the shear stress; thus, when the synthetic jets are activated the dc level of the shear stress sensor is much lower than that of the uncontrolled case (12a), which is indicative of increase of the shear, as expected when the flow is reattached. From the shear stress data it was concluded that either the sensor's dc level or its rms (or both) can be used to detect separation. In the present work we used the rms as the separation indicator.

From the data in Figs. 11–13 it is clear that a stall detection system can be implemented simply by continuously monitoring the rms of the shear stress sensor reading. Thus, a simple closed-loop stall suppression system was implemented by choosing a threshold rms value which, if reached, will trigger the activation of the synthetic jets to reattach the flow. In what follows, the angle of attack was slowly increased until stall occurred. Then, based on the rms threshold criterion, the synthetic jets were automatically activated through a D/A board, using a LabVIEW code.

Figures 14a–14c present the time trace of the shear stress sensor output as the angle of attack increases monotonically for different rms thresholds. Note that in these figures the time axis has been arbitrarily set to zero when the flow is on the verge of separation from the airfoil's upper surface. In the first experiment, the rms threshold was set to 0.5 V (Fig. 14a). As time progresses (i.e., as the angle of attack increases) the shear stress output voltage increases (corresponding to a decrease in the shear stress). When the angle of attack is ~ 8 deg ($t = 0$) the flow separates, which is indicated by the increase in the rms as well as by the jump in shear stress reading (marked by the arrow). It takes about 2.5 s before the control is triggered and the synthetic jets are activated, resulting in a complete flow reattachment, as indicated by the significant decrease in the shear stress sensor output voltage. The figure also includes a sketch of the roll moment (from the sting balance reading), which shows that when the flow is separated a roll moment is generated (due to a slight asymmetry of the model that yields an asymmetric flow separation on the wings). When the synthetic jets are activated the roll moment diminishes due to flow reattachment on both wings, resulting in a symmetric flow over the wingtips.

Next, the rms threshold was reduced to 0.25 V (Fig. 14b). Again, the flow separates and it takes ~ 0.5 s before the synthetic jets are activated (compared to 2.5 s for the 0.5 V rms threshold case). When the rms threshold is reduced to 0.1 V (Fig. 14c), the threshold was reached *before the wingtips ever stalled*. This suggests that through the selection of an appropriate shear stress rms threshold, synthetic jets can not only recover a wing from stall, but avoid it altogether. Furthermore, a roll moment is not generated.

Dynamic Model

As part of the development of closed-loop control system, the dynamic response of the model following the activation of the synthetic jet is required. Here, the analysis was conducted on an RC flying Cessna 182 model (1.65 m span and 1.27 m total length) based on the scaled wind tunnel model data. Ideally, the dynamic response is found by measuring the aerodynamic force and moment responses. However, this requires dynamic force/torque sensors, which were not available for these tests. Instead, the shear stress sensor output was used, which indicates the state of the flow and is closely related to aerodynamic forces and moments. Thus, the dynamic response of the shear stress sensor was used to characterize the aerodynamic response of the entire vehicle. Experiments were conducted to determine the dynamic response of the shear stress when a step input to the synthetic jets was applied. The signal was on for 0.5 s and off for 0.5 s and the transient response of the shear stress following the activation and termination of the synthetic jets was measured by phase locking the data acquisition to the onset of the synthetic jets' input signal.

A typical response of the shear stress sensor to the step input signal is presented in Figs. 15a and 15b (the onset and termination times of

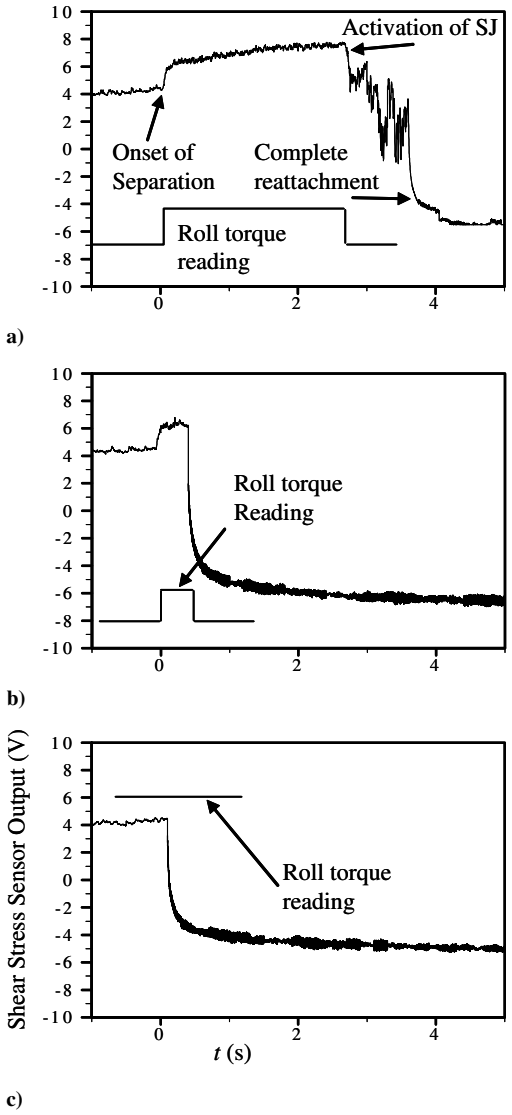

Fig. 14 Change of the shear stress sensor output with time (as the angle of attack increases). a) rms = 0.5, b) 0.25, and c) 0.1 V.

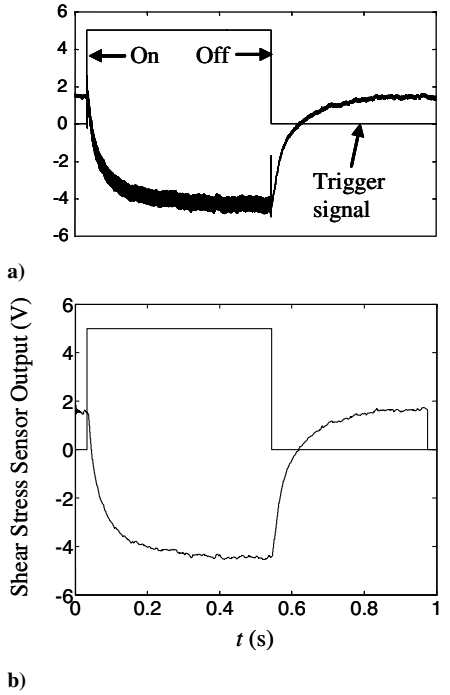

Fig. 15 Response of the shear stress sensor output following the activation and termination of the synthetic jets. $\alpha = 12$ deg, $C_\mu = 8.6 \times 10^{-3}$, $Re = 134,600$. a) Unfiltered; b) filtered.

the synthetic jets are marked on the trigger signal). In these experiments the angle of attack is 12 deg and the Reynolds number is 134,600. At this angle of attack the flow over the wingtips is separated and the activation of the control results in a decrease in the shear stress sensor output voltage (which corresponds to an increase in the shear). It takes about 0.3 s for the flow to completely reattach to the surface (following the activation of the synthetic jets) and about the same time for the flow to reseparate once the synthetic jets are turned off. Note that the response of the shear stress sensor resembles that of a first-order system. Furthermore, the sensor response has a component of the synthetic jet driving signal frequency (750 Hz) and its harmonics. Therefore, in the analysis conducted here, a low pass filter with cutoff frequency at 400 Hz was implemented (Fig. 15b). Note that the time-averaged shear stress varies for different wind tunnel speeds, angles of attack, and different input signals; however, its transitory behavior in all experiments conducted is very similar. The response of the shear stress to the activation of the synthetic jets can be described as a first-order system as follows:

$$\frac{1}{TS+1} \tag{1}$$

where T is the time constant.

From the experimental data, the time constant T is approximated by the time it takes the shear stress sensor reading to reach 63% of its final value, which, in the present experiments, is $T \approx 0.04$ s. Note that this time definition is commonly used in dynamic stability analysis. Furthermore, the characteristic time of the flow (i.e., the time of flight, $T_f = \bar{c}/U_\infty$) is 0.026 and 0.052 s for Reynolds numbers of 67,300 and 134,600, respectively. Therefore, the time constant for the reattachment and reseparation (using synthetic jet actuators) can be approximated by the characteristic time of the flow.

From the wind tunnel experiments, the synthetic jet wingtip model can be described as

$$\Delta C_r = f_r(V)\frac{1}{TS+1} \tag{2}$$

$$\Delta C_n = f_n(V)\frac{1}{TS+1} \tag{3}$$

where $f_r(V)$ and $f_n(V)$ are functions presented in Eqs. (4) and (5), respectively, and V is the input voltage to the port wing's synthetic jets.

$$\Delta C_r = f_r(V) = 0.016V - 0.0102V^2 + 0.0027V^3 \tag{4}$$

$$\Delta C_n = f_n(V) = -0.2164 \times 10^{-3}V - 0.294 \times 10^{-3}V^2 + 0.2349 \times 10^{-3}V^3 \tag{5}$$

From the preceding approximations a high fidelity dynamic model for both the baseline Cessna and the Cessna with synthetic jet wingtips was developed and implemented in Simulink. Note that the values are scaled up to a 1.65 m wing span RC Cessna model, which will be used in the future as the testbed for the technology presented in this paper. The structure of the simulation model is illustrated in Fig. 16. The aerodynamic coefficients that were not measured in the wind tunnel experiments were approximated by a mathematical model of a Cessna 182 [15], and they will be replaced in the future with empirical data when additional experiments are conducted.

The 6-DOF Cessna dynamic model (Fig. 16) is described by Eqs. (6–15) for the rotational and translational dynamics, respectively.

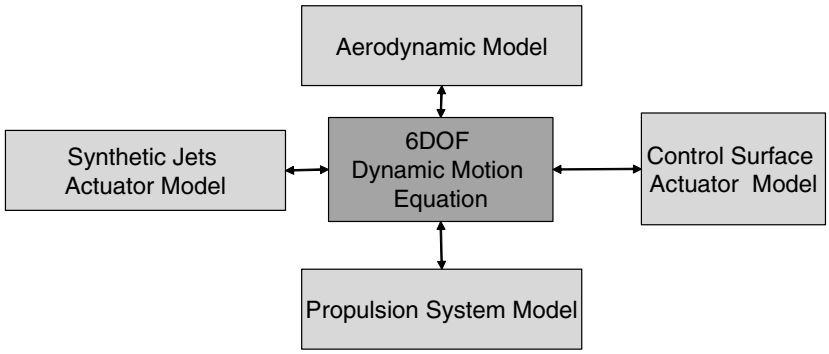

Fig. 16 Cessna's 6-DOF dynamic model.

$$\dot{\phi} = p + q\sin(\phi)\tan(\theta) + r\cos(\phi)\tan(\theta) \tag{6}$$

$$\dot{\theta} = q\cos(\phi) - r\sin(\phi) \tag{7}$$

$$\dot{\psi} = \sin(\phi)\sec(\theta) + r\cos(\phi)\sec(\theta) \tag{8}$$

$$\dot{p} = I^p_{pq}pq + I^p_{qr}qr + g^p_l T_l + g^p_n T_n \tag{9}$$

$$\dot{q} = I^q_{pp}p^2 + I^q_{rr}r^2 + I^q_{pr}pr + g^q_m T_m \tag{10}$$

$$\dot{r} = I^r_{pq}pq + I^r_{qr}qr + g^r_l T_l + g^r_n T_n \tag{11}$$

$$\dot{u} = \frac{1}{m}(F_x - mgS_\theta) - qw + rv \tag{12}$$

$$\dot{v} = \frac{1}{m}(F_y + mgC_\theta S_\phi) - ru + pw \tag{13}$$

$$\dot{w} = \frac{1}{m}(F_z + mgC_\theta C_\phi) - pv + qu \tag{14}$$

$$\begin{bmatrix}\dot{x}\\ \dot{y}\\ \dot{z}\end{bmatrix} = \begin{bmatrix}C_\theta C_\psi & S_\phi S_\theta S_\psi - C_\phi S_\psi & C_\phi S_\theta C_\psi + S_\phi S_\psi\\ C_\theta S_\psi & S_\phi S_\theta S_\psi + C_\phi C_\theta & C_\phi S_\theta S_\psi - S_\phi C_\psi\\ -S_\theta & S_\phi C_\theta & C_\phi C_\theta\end{bmatrix}\begin{bmatrix}u\\ v\\ w\end{bmatrix} \tag{15}$$

Figure 17 presents the diagram of the Simulink simulation model. The actuator commands refer to engine δ_{Th}, aileron δ_a, elevator δ_E, and rudder δ_R commands for the baseline configuration. For the synthetic jets configuration, the aileron command is replaced by an input voltage δ_{SV}, where δ_{SV} is defined as

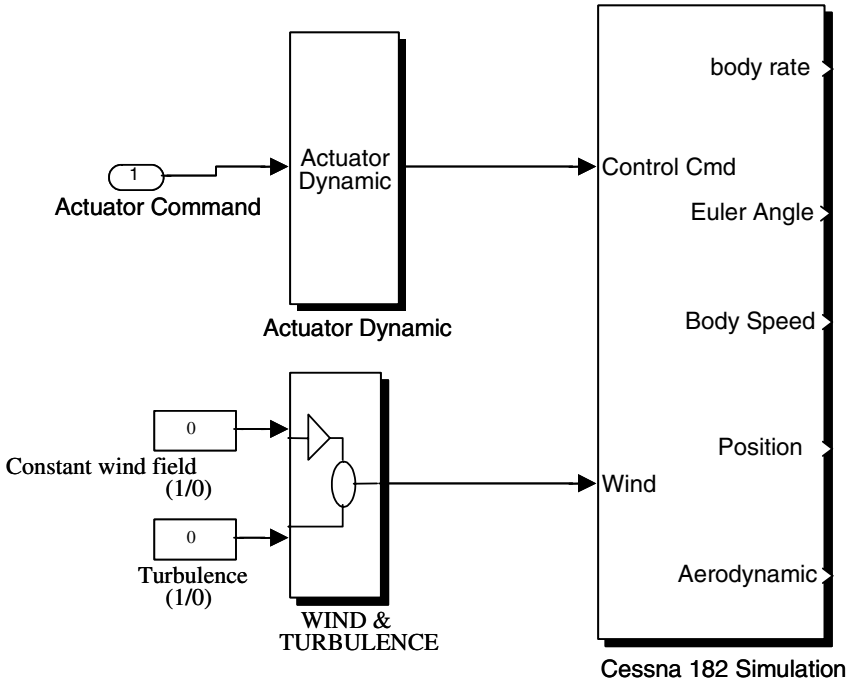

Fig. 17 Diagram of the Simulink simulation model for the RC Cessna.

Table 1 Actuator simulation time constants

	Time constants, s
Aileron	0.06
Elevator	0.06
Rudder	0.06
Synthetic jet wingtips	0.075
Engine	0.6

Table 2 Controller parameters

Command filter and controller closed-loop characteristic bandwidth	Proportional gain (Kp)	Integral Gain (KI)
P channel 2	2.828	4
q channel 1	1.414	1
r channel 1	1.414	1

$$\delta_{SV} \in [-5, 5] \text{ V} \tag{16}$$

If $\delta_{SV} > 0$ the starboard wingtip jets are activated with an input voltage, and the port wingtip jets are off. If $\delta_{SV} < 0$ the port wingtip jets are switched on with an input voltage of $-\delta_{SV}$, and the starboard wingtip jets are off.

In this simulation system, at high angles of attack, the aileron coefficients for the baseline case are represented by spline functions, obtained from the experiments. The propulsion model is described as Thrust $= \delta_{\text{Th}}$ mg, where δ_{Th} is the unitless number representing the throttle setting for the engine.

The dynamics of actuators are approximated by independent first-order systems with time constants, whereas aileron, elevator, and rudder time constants are estimated from servo motor properties and are presented in Table 1. The synthetic jet wingtips' time constant is scaled up from the experimental results to the flying model scale (having 1.5 m wing span).

Integrated Flight Control with Flow Control System

Based on the Cessna dynamic model, an integrated flight controller (body rate controller) was designed for the Cessna that is instrumented with synthetic jet wingtips. A body rate controller is the basic building block for a future autonomous flight control system. The designed body rate controller can follow a given command by employing the synthetic-jets-controlled wingtips, rudder, and elevator.

The structure of the control system is illustrated in Fig. 18. The nominal controller is based on feedback linearization. It is augmented by an adaptive neural network controller to compensate for the model uncertainty. In the current simulation model, it is found that the nominal controller by itself is very robust, thus the neural

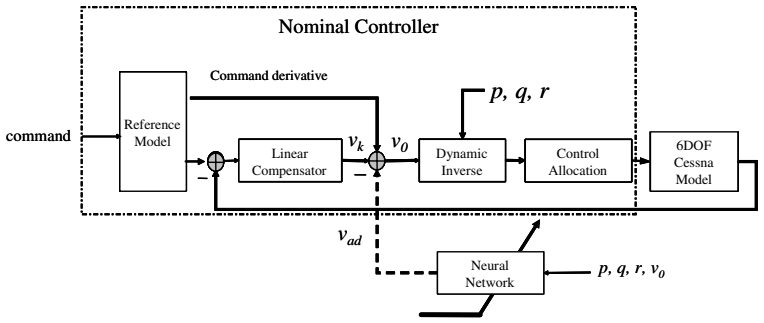

Fig. 18 Structure of the closed-loop control system.

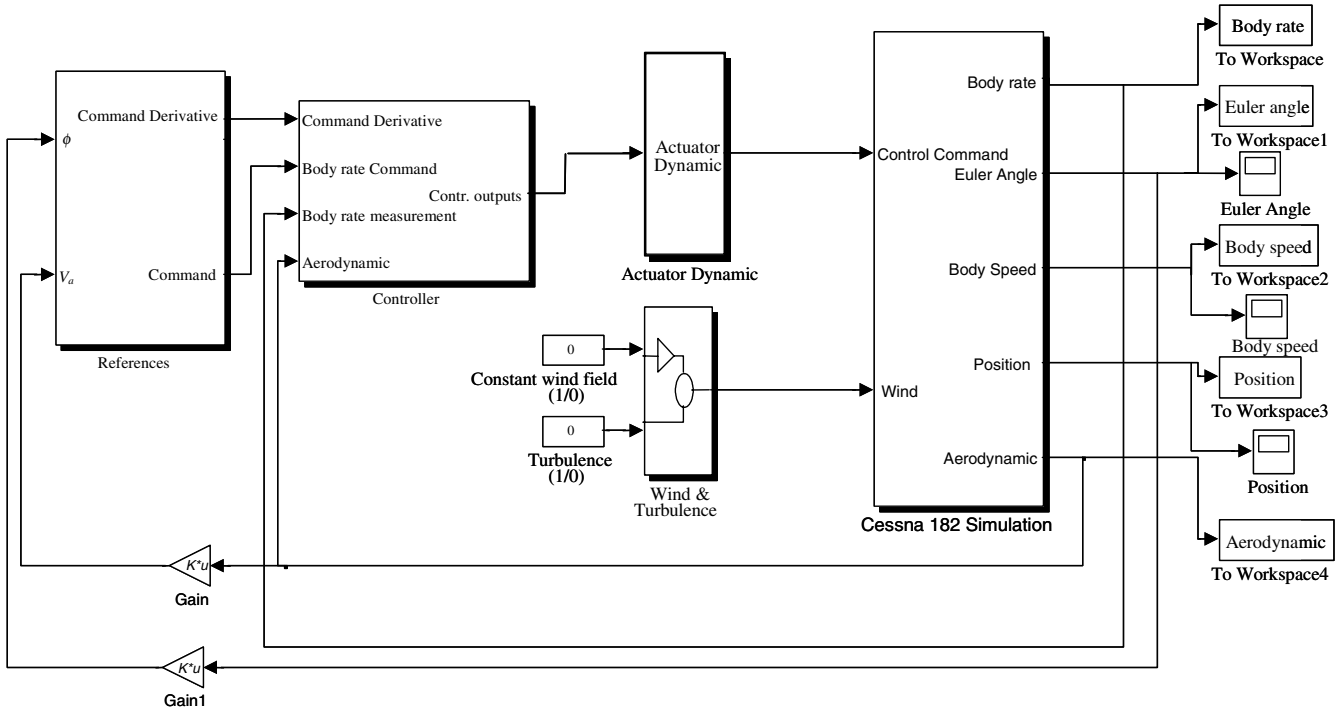

Fig. 19 Simulink simulation of the integrated flight control using synthetic jets.

network adaptive controller was not engaged. It is also worth noting that although the controller is only for body rate, the full 6-DOF dynamics is simulated to evaluate the controller performance.

The Cessna body rate dynamics can be rewritten as

$$\dot{p} = I^p_{pq} pq + I^p_{qr} qr + g^p_l (T_{l_{\text{aero}}} + T_{l_{\text{ctrl}}}) + g^p_n (T_{n_{\text{aero}}} + T_{n_{\text{ctrl}}}) \quad (17)$$

$$\dot{q} = I^q_{pp} p^2 + I^q_{rr} r^2 + I^q_{pr} pr + g^q_m (T_{m_{\text{aero}}} + T_{m_{\text{ctrl}}}) \quad (18)$$

$$\dot{r} = I^r_{pq} pq + I^r_{qr} qr + g^r_l (T_{l_{\text{aero}}} + T_{l_{\text{ctrl}}}) + g^r_n (T_{n_{\text{aero}}} + T_{n_{\text{ctrl}}}) \quad (19)$$

where the applied torques are divided into two parts: the aerodynamic torques on the wing-body, $T_{l_{\text{aero}}}$, $T_{m_{\text{aero}}}$, and $T_{n_{\text{aero}}}$, which are not related to actuator control input and engine thrust generated torque, and the actuator generated torques, $T_{l_{\text{ctrl}}}$, $T_{m_{\text{ctrl}}}$, and $T_{n_{\text{ctrl}}}$. The nominal controller design can be described by the following two parts.

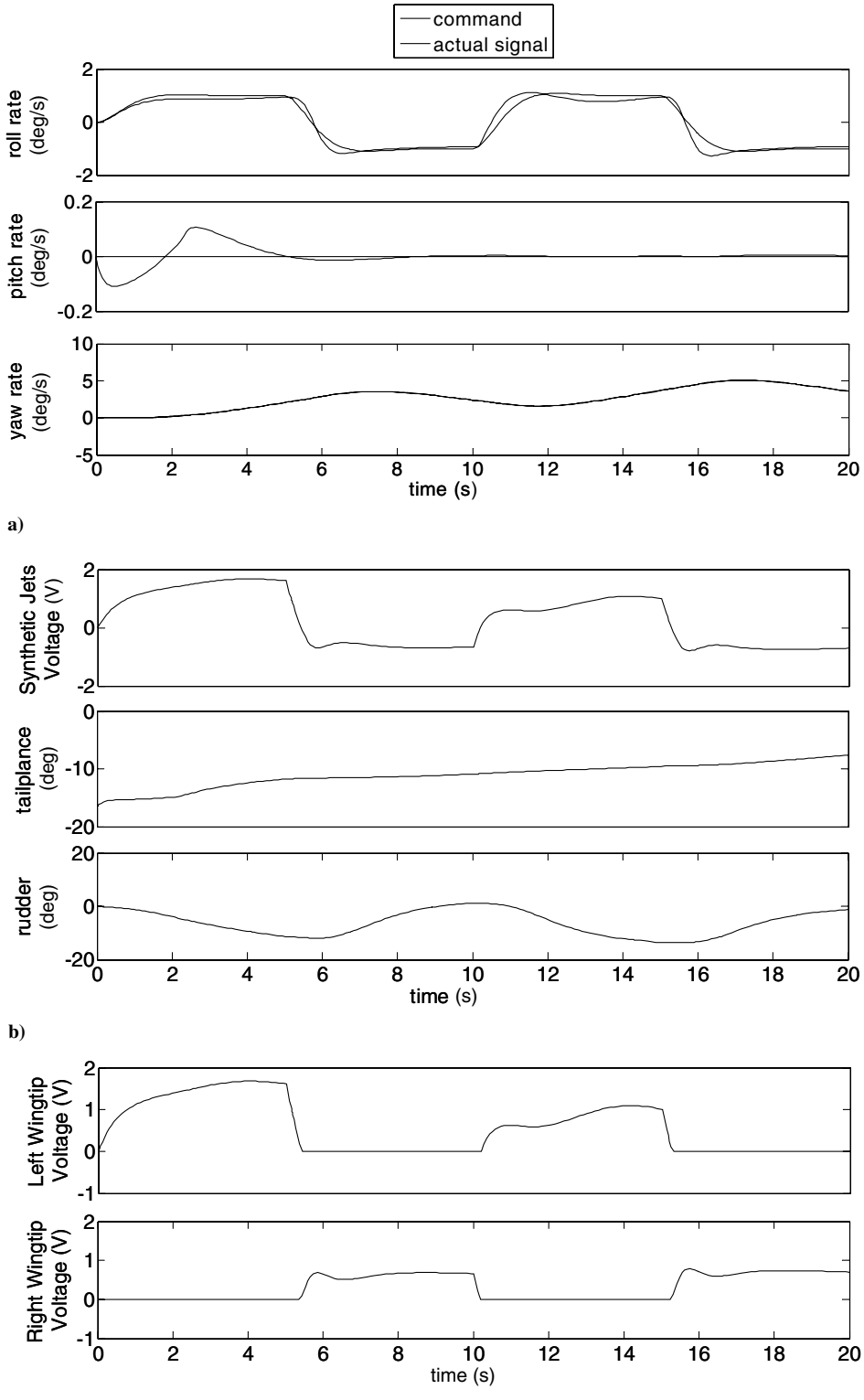

Fig. 20 Simulation results of a coordinated turn during the approach. a) Body rate command and response, b) actuator commands to the synthetic jets, elevator, and rudder, and c) input voltage to each of the wingtips.

Feedback Linearization Based Control Design

$$\begin{bmatrix} T_{l_{\text{ctrl}}} \\ T_{m_{\text{ctrl}}} \\ T_{n_{\text{ctrl}}} \end{bmatrix} = \begin{bmatrix} g_l^p & 0 & g_n^p \\ 0 & g_m^q & 0 \\ g_l^r & 0 & g_n^r \end{bmatrix} \begin{bmatrix} -(I_{pq}^p pq + I_{qr}^p qr) + \dot{p}_c - k_p\tilde{p} - k_{pI}\tilde{p}_I \\ -(I_{pp}^q p^2 + I_{rr}^q r^2 + I_{pr}^q pr) + \dot{q}_c - k_p\tilde{q} - k_{qI}\tilde{q}_I \\ -(I_{pq}^r pq + I_{qr}^r qr) + \dot{r}_c - k_c\tilde{r} - k_{rI}\tilde{r}_I \end{bmatrix} - \begin{bmatrix} T_{l_{\text{aero}}} \\ T_{m_{\text{aero}}} \\ T_{n_{\text{aero}}} \end{bmatrix} \tag{20}$$

where p_c, q_c, and r_c are body rate commands, $\tilde{p} = p - p_c$, $\tilde{q} = q - q_c$, $\tilde{r} = r - r_c$ are tracking errors, $\tilde{p}_I = \int_0^t \tilde{p}$, $\tilde{q}_I = \int_0^t \tilde{q}$, $\tilde{r}_I = \int_0^t \tilde{r}$ are integral tracking errors, k_p, k_{pI}, k_q, k_{qI}, k_r, and k_{rI} are feedback gains. Therefore, the body rate closed-loop controller has the following characteristics equations:

$$\begin{bmatrix} \lambda^2 + k_p\lambda + k_{pI} \\ \lambda^2 + k_q\lambda + k_{qI} \\ \lambda^2 + k_r\lambda + k_{rI} \end{bmatrix} = \begin{bmatrix} 0 \\ 0 \\ 0 \end{bmatrix} \tag{21}$$

Controller Allocation

From the rotation dynamic equations, one can derive the following equation:

$$\begin{bmatrix} T_{l_{\text{ctrl}}} \\ T_{m_{\text{ctrl}}} \\ T_{n_{\text{ctrl}}} \end{bmatrix} = C_A \begin{bmatrix} \delta_{SV} \\ \delta_T \\ \delta_R \end{bmatrix} \tag{22}$$

where C_A is the controller allocation matrix obtained from the actuator model. Thus, the actuator command can be calculated as

$$\begin{bmatrix} \delta_{SV} \\ \delta_T \\ \delta_R \end{bmatrix} = C_A^{-1} \begin{bmatrix} T_{l_{\text{ctrl}}} \\ T_{m_{\text{ctrl}}} \\ T_{n_{\text{ctrl}}} \end{bmatrix} \tag{23}$$

In the controller design process, the coefficients for the synthetic jet configuration [Eqs. (4) and (5)] are simplified as follows:

$$\Delta C_r = 0.0098\delta_{SV} \tag{24}$$

$$\Delta C_n = 0 \tag{25}$$

The controller parameters are shown in Table 2. Note that by comparing the controller closed-loop bandwidth, the actuator time constant (shown in Table 2) is fast enough. The bandwidth of the actuator is more than three times faster than the desired controller closed-loop bandwidth. Thus, the actuator dynamics can be ignored in the controller design process. The model error induced by this simplification during controller design process can be compensated for by the closed-loop control, which is verified in the simulation results. The Simulink simulation of integrated flight control using synthetic jets is shown in Fig. 19.

Simulation Results of Integrated Flight Control and Flow Control

The simulation of integrated flight control and flow control has been tested for a scenario in which the Cessna is approaching the runway for landing at an angle of attack of 10 deg. Using the trim program of the simulation model, the trim condition is $\delta_e = -0.288$ rad, $\delta_{\text{Th}} = 0.162$, $u_b = 11.67$ m/s, $w_b = 1.15$ m/s. The command in a coordinated turn during approach is given by

$$r_{\text{command}} = \frac{g\tan(\phi)}{V_a} \tag{26}$$

Figure 20 shows the simulation results of a coordinated turn during the approach. Figure 20a shows the body rate command and response, Fig. 20b presents an actuator command to the synthetic jets, elevator, and rudder, whereas Fig. 20c shows the input voltage to each of the wingtips. These simulation results show that the synthetic jet wingtips are able to replace traditional ailerons and provide enough control authority for roll control (at least for the example maneuver presented here). It is worth noting that during the controller design, the synthetic jet configuration's coefficients were replaced by a very simplified model and that the closed-loop flight control is robust enough to the handle the error introduced by the controller design process.

Summary

The application of active flow control, via synthetic jets actuators, for separation control and roll control has been tested in wind tunnel experiments. Using synthetic jets, mounted in the wingtips, delays separation by ~2 deg whereas the maximum lift coefficient is increased by up to 15%. It was shown that synthetic jets can provide similar control authority as conventional ailerons, where proportional control in pitch and roll was achieved for angles of attack larger than 6 deg.

The rms output of a shear stress sensor was used to detect separation on the wingtips of a scaled Cessna 182 model. This detection technique was integrated with a computer and synthetic jet actuators to create a simple closed-loop stall suppression system. To the authors' knowledge this is the first time that such a system ever developed for a plane model.

Using the wind tunnel data, an analysis of the dynamic response of an RC scale model of a Cessna 182 was performed and an integrated flight control with flow control was developed. The next logical step is to instrument an RC model with synthetic jets along the wingtips and attempt roll control in flight using only synthetic jet actuators.

Acknowledgments

This work was supported as part of SBIR phase I, Contract Number FA8650-05-M-3539, monitored by John Casey and James Myatt. The authors would also like to thank Eric White from RPI, who assisted in running all of the wind tunnel experiments, and Frank (Xiaodong) Zhang from IAI for his contribution in the early stages of the work.

References

[1] Wentz, W. H., Jr., "Effectiveness of Spoilers on the GA(W)-1 Airfoil with a High Performance Fowler Flap,". NASA CR-2538, 1975.

[2] Ahuja, K. K., and Burrin, R. H., "Control of Flow Separation by Sound," AIAA Paper 1984-2298, 1984.

[3] Zaman, K. B. M. Q., Bar-Sever, A., and Mangalam, S. M., "Effect of Acoustic Excitation on the Flow over a Low-Re Airfoil," *Journal of Fluid Mechanics*, Vol. 182, Sept. 1987, pp. 127–148.

[4] Hsioa, F. B., Liu, C. F., and Shyu, J-Y. "Control of Wall-Separated Flow by Internal Acoustic Excitation," *AIAA Journal*, Vol. 28, No. 8, 1990, pp. 1440–1446.

[5] Neuberger, D., and Wygnanski, I., "The Use of a Vibrating Ribbon to Delay Separation on Two Dimensional Airfoils," *Proceedings of Air Force Academy Workshop on Unsteady Separated Flow*, Rept. TR-88-000, 1987.

[6] Seifert, A., Darabi, A., and Wygnanski, I., "Delay of Airfoil Stall by Periodic Excitation," *Journal of Aircraft*, Vol. 33, No. 4, 1996, pp. 691–698.

[7] Smith, B. L., and Glezer, A., "The Formation and Evolution of Synthetic Jets," *Physics of Fluids*, Vol. 10, No. 9, 1998, pp. 2281–2297.

[8] Amitay, M., and Glezer, A., "Controlled Transients of Flow Reattachment over Stalled Airfoils," *International Journal of Heat and Fluid Flow*, Vol. 23, No. 5, 2002, pp. 690–699.

[9] Amitay, M., and Cannelle, F., "Evolution of Finite Span Synthetic Jets," *Physics of Fluids*, Vol. 18, No. 054101, 2006.

[10] Amitay, M., Smith, B. L., and Glezer, A., "Aerodynamic Flow Control Using Synthetic Jet Technology," AIAA Paper 1998-0208, 1998.

[11] Amitay, M., Smith, D. R., Kibens, V., Parekh, D. E., and Glezer, A., "Modification of Lifting Body Aerodynamics Using Synthetic Jet Actuators," *AIAA Journal*, Vol. 39, No. 3, 2001, pp. 361–370.

[12] Amitay, M., Pitt, D., and Glezer, A., "Separation Control in Duct Flows," *Journal of Aircraft*, Vol. 39, No. 4, 2002, pp. 616–620.

[13] Morel-Fatio, S., Pines, D. J., Kiddy, J., "UAV Performance Enhancements with Piezoelectric Synthetic Jet Actuators," AIAA Paper 2003-394, 2003.

[14] Amitay, M., Horvath, M., Michaux, M., and Glezer, A., "Virtual Aerodynamic Shape Modification at Low Angles Attack Using Synthetic Jet Actuators," AIAA Paper 2001-2975, 2001.

[15] Roskam, J., *Airplane Flight Dynamics and Automatic Flight Controls*, DAR Corporation, Lawrence, KS, 1995.